Nature and evolution of the lithospheric mantle beneath the passive margin of East Oman: evidence from mantle xenoliths sampled by Cenozoic alkaline lavas

Michel Grégoire, Jessica Langlade, Guillaume Delpech, Céline Dantas, Georges Ceuleneer

Elsevier Editorial System(tm) for Lithos
Manuscript Draft

Manuscript Number:

Title: Nature and evolution of the lithospheric mantle beneath the passive margin of East Oman: evidence from mantle xenoliths sampled by Cenozoic alkaline lavas

Article Type: Research Paper

Section/Category:

Keywords: Oman; upper mantle; xenoliths; harzburgites; lherzolites; trace elements; metasomatism; Owen basin

Corresponding Author: Dr. Michel Gregoire, Ph.D.

Corresponding Author's Institution: CNRS-Observatoire Midi Pyrenees

First Author: Michel Gregoire, Ph.D.

Order of Authors: Michel Gregoire, Ph.D.; Michel Gregoire; Jessica Langlade; Guillaume Delpech; Celine Dantas; Georges Ceuleneer

Manuscript Region of Origin:

Abstract: Cenozoic alkaline lavas from the Al Ashkharah area, facing the Indian ocean along the North-East Oman coastline, contain numerous small (< 2cm) mantle xenoliths. They provide a unique opportunity to investigate the nature and evolution of the upper mantle beneath the Oman passive margin, bordering the Owen Basin. All studied xenoliths are porphyroclastic to equigranular spinel lherzolites and harzburgites They are all devoid of amphibole and phlogopite. The composition of their clinopyroxenes, orthopyroxenes, olivines and spinels indicate that these samples are witnesses of a typical subcontinental lithospheric upper mantle and are quite distinct from the peridotites cropping out in the nearby Oman ophiolite.
The clinopyroxene major element composition record an evolution from fertile lherzolites (Mg#: 89 and Al2O3: 7.5 wt%) to refractory harzburgites (Mg#: 93.5 and Al2O3: 2.5 wt%). The clinopyroxene of most samples are characterised by REE patterns evolving continuously from spoon-shaped to LREE-enriched with almost flat HREE spectra (LaN/YbN: 2.5-30; LaN/SmN: 3.2-24; SmN/YbN: 0.25-4.6; HoN/LuN : 0.88-1.15) and strong negative Ba, Nb, Zr, Hf and Ti anomalies. We propose that these geochemical fingerprints can be accounted for in the frame of a two stages; (1) a - likely ancient - decompression melting event characterised by a degree ranging from 1 to a maximum of 19 % and unrelated to the recent tectonic evolution of the Oman margin, followed by (2) metasomatic transformation possibly related to the circulation of carbonate-rich silicate melt during the Cenozoic rifting event that led to the opening of the Owen basin.

Nature and evolution of the lithospheric mantle beneath the passive margin of East Oman: evidence from mantle xenoliths sampled by Cenozoic alkaline lavas

Grégoire[1*], M., Langlade[1], J.A., Delpech, G.[2], Dantas[1], C. and Ceuleneer[1], G.

1. CNRS-UMR 5562 DTP :Dynamique Terrestre et Planétaire. Observatoire Midi Pyrénées, Université Paul Sabatier,14 Avenue. E. Belin, 31400 Toulouse, France.

2. UMR CNRS 8148 IDES : Interactions et Dynamique des Environnements de Surface, Faculté des Sciences, Université Orsay-Paris Sud, Bât.504, 91405 ORSAY Cedex, France

- * : Corresponding author : michel.gregoire@dtp.obs-mip.fr
  Tel: +33 5 61 33 29 77; Fax: +33 5 61 33 29 00

Abstract

Cenozoic alkaline lavas from the Al Ashkharah area, facing the Indian ocean along the North-East Oman coastline, contain numerous small (‹ 2cm) mantle xenoliths. They provide a unique opportunity to investigate the nature and evolution of the upper mantle beneath the Oman passive margin, bordering the Owen Basin. All studied xenoliths are porphyroclastic to equigranular spinel lherzolites and harzburgites They are all devoid of amphibole and phlogopite. The composition of their clinopyroxenes, orthopyroxenes, olivines and spinels indicate that these samples are witnesses of a typical subcontinental lithospheric upper mantle and are quite distinct from the peridotites cropping out in the nearby Oman ophiolite.

The clinopyroxene major element composition record an evolution from fertile lherzolites (Mg#: 89 and Al_2O_3: 7.5 wt%) to refractory harzburgites (Mg#: 93.5 and Al_2O_3: 2.5 wt%). The clinopyroxene of most samples are characterised by REE patterns evolving continuously from spoon-shaped to LREE-enriched with almost flat HREE spectra (La_N/Yb_N: 2.5-30; La_N/Sm_N: 3.2-24; $Sm_N/Yb_{N:}$ 0.25-4.6; Ho_N/Lu_N : 0.88-1.15) and strong negative Ba, Nb, Zr, Hf and Ti anomalies. We propose that these geochemical fingerprints can be accounted for in the frame of a two stages; (1) a - likely ancient - decompression melting event characterised by a degree ranging from 1 to a maximum of 19 % and unrelated to the recent tectonic evolution of the Oman margin, followed by (2) metasomatic transformation possibly related to the circulation of carbonate-rich silicate melt during the Cenozoic rifting event that led to the opening of the Owen basin.

Key words

Oman; upper mantle; xenoliths; harzburgites; lherzolites; trace elements; metasomatism; Owen basin.

Introduction

Mantle xenoliths brought to the surface by alkaline magmas provide a direct access to the petrological processes conditioning the nature and evolution of the upper mantle (e.g. Coltorti et al., 1999 ; Grégoire et al., 1997 and 2000 ; Delpech et al., 2004). Mantle xenoliths from continental rift systems have been largely studied all around the world in the last decades (e.g. Ionov et al., 2002; Witt-Eickschen et al., 2003 ; Lenoir et al., 2000). Small (< a few cm), mostly lherzolitic, xenoliths have been recently discovered in alkaline dykes and flows emplaced during Cenozoic times along the Oman passive margin facing the Owen basin (see Gnos and Peters, 2003) but they have not been extensively studied yet for their trace element geochemistry. Nasir et al. (2006) report on bulk rock trace element analyses but, given the small size of the xenoliths, contamination with the host lava cannot be excluded. Among other, the marked enrichment in incompatible elements they observed might not be related to mantle processes. The present paper is a complementary study to the one of these authors in terms of analytical procedure: we performed *in situ* (LA-ICP-MS) determinations of the trace element content of clinopyroxene to avoid at best the risk of contamination with the host alkaline lavas. Moreover, we sampled some localities not studied by Nasir et al. (2006) and the lithological diversity of our collection appears to be more pronounced. The question addressed in the present paper concerns the nature of the upper mantle beneath the

eastern Oman mountains, among other how does it compare to the peridotites cropping out in the Semail ophiolite, relics of the sub-oceanic mantle from a nearby area. Our aim is also to decipher if the upper mantle beneath the Oman margin was affected by the melting and/or melt migration processes related to the Cenozoic rifting of the Owen basin. We compare our results to those from the studies of the mantle peridotite xenoliths from Spitsbergen (Ionov et al., 2002; Gregoire et al., submitted). Indeed the latter come from the same kind of setting (rift-zones) and display close similarities with the xenoliths studied here.

Geological setting and sampling

The building and present structure of the Northern Oman mountains result essentially from the obduction of the Semail ophiolite during Maestrichtian times and from a regional uplift that started during the Miocene (Glennie et al, 1974; Coleman, 1981). Our study area is located at the eastern termination of this domain, along a major structural lineament referred to as the Masirah fault (Moseley, 1969). The Masirah line acted as a major transform plate boundary that accommodated the northward drift of the Indian continental block during Cretaceous and Paleocene times (e.g. Royer et al, 2002; Fournier et al, 2008). As a result of the kinematic reorganization that followed the India-Eurasia collision (about 52 Ma ago, Patriat and Achache, 1984), this transform boundary shifted into its present “off shore” position along the Owen Fracture Zone.

Although this general picture is reasonably well understood, the precise evolution of the Eastern Oman margin during the late Cretaceous and early Cenozoic times was rather complex and is still poorly constrained. Regional geolological studies have

shown that long transtensive periods alternated with shorter transpressive ones (e.g. Platel and Roger, 1989). The best documented of these transpressive “events” occurred during upper Maastrichtian lower Paleocene times; it is witnessed by the oblique thrusting of sedimentary nappes and by the obduction of the Masirah ophiolite, a piece of upper Jurassic oceanic lithosphere that likely evolved in a ridge-transform tectonic setting during the accretion of the proto-Indian ocean (Gnos and Perrin, 1995; Gnos et al, 1997; Peters and Mercolli, 1998). Since Eocene times, the coast of East Oman behaved like a passive margin bordering a rift zone that eventually led to the opening of the Gulf of Aden (Platel and Roger, 1989). The opening of the Owen basin is possibly one of the events that complicated the evolution of this margin, although the age of the oceanic crust in the Owen basin is still debated (Fournier et al, 2008). Current structural and kinematic studies, among other around the Aden-Owen-Carlsberg triple junction will result in a better understanding of the evolution of this area (J.-Y. Royer, pers. com.).

Alkaline magmatism that affected the East Oman margin seems to belong to two main eruptive events: a first one contemporaneous with the compressive stage that affected the area at the Cretaceous-Tertiary boundary, and more recent dyke injections during the Eocene extension.

Mantle xenoliths studied in the present study were sampled in five occurrences of these N-S to NNE-SSW trending tertiary dykes in the Al Ashkarah area (Figure 1). Their precise age is poorly constrained: the dykes cross-cut Paleocene sediments but not more recent Eocene ones. Ar/Ar ages ranging from about 36 to 40 Ma have been published by Worthing and Wilde (2002) for the dykes including our samples of mantle xenoliths showing that they belong to the second, Eocene, injection event.

Analytical methods

Major and trace elements of minerals were analysed at the UMR 5563 (LMTG, Observatoire Midi-Pyrénées) of University Paul Sabatier (Toulouse III).

Major-element compositions of minerals were determined with the CAMECA SX50 electron microprobe and a standard program: beam current of 20nA and acceleration voltage of 15 kV, 10 to 30s/peak, 5-10s/background counting times, and natural and synthetic minerals as standards. Nominal concentrations were subsequently corrected using the PAP data reduction method (Pouchou and Pichoir, 1984). The theoretical lower detection limits are about 100 ppm (0,01%).

The concentrations of Rare Earth Elements and other trace elements (La, Ce, Pr, Nd, Sm, Eu, Gd, Tb, Dy, Ho, Er, Yb, Lu, Rb, Ba, Th, Sr, Zr, Ti, Y, Ni, V and Sc) in clinopyroxenes were analysed in situ on >120 mm thick polished sections with a Perkin-Elmer Elan 6000 ICP-MS instrument coupled to a CETAC laser ablation module that uses a 266 nm frequency-quadrupled Nd-YAG laser. The NIST 610 and 612 glass standards were used to calibrate relative element sensitivities for the analyses. The analysis were normalized using CaO values determined by electron microprobe. The analyses were performed on inter-clivage area from the cores of the freshiest cpx grains in order to get homogeneous results unaffected by alteration or exsolution processes. A beam diameter of 50-100 μm and a scanning rate of 20 μm/s were used. The typical relative precision and accuracy for a laser analysis range from 1 to 10%. Typical theoretical detection limits range from 10 to 20 ppb for REE, Ba, Rb, Th, Sr, Zr and Y; 100ppb for Sc and V; and 2 ppm for Ti and Ni (see in Dantas et al., 2007 for more details).

Petrography

The lavas hosting the ultramafic xenoliths are microlitic basalts. The xenoliths being small, < 2cm in size (Figure 2), it has been difficult to define the rock-types unambiguously. Nevertheless, wedistinguished two main rock types: (i) spinel lherzolites (samples 04OM58a2, 04OM58a3, 04OM58c3, 04OM58f3, 04OM59b2, 04OM62b2, 04OM63c2, and 04OM66d2); and (ii) spinel harzburgites (samples 04OM58b1, 04OM62b1, 04OM63a1, 04OM63a2, 04OM63c1 and 04OM63c3). None of the xenoliths display amphibole or phlogopite. All the peridotites correspond to mantle peridotites equilibrated in the spinel stability field. Considering the small size of the xenoliths, the following modal compositions are only indicative.

The peridotites are relatively fresh, the serpentinisation of the olivine and the orthopyroxene being always limited. Some clinopyroxenes and particularly those from sample 04OM62b2, show spongy textures commonly limited to the rim but sometimes affecting the entire crystal. The formation of this type of texture is probably related to local melting process affecting the clinopyroxenes during the transport of the xenoliths to the surface by the host-lavas (e.g. Grégoire et al., 2000, Carpenter et al., 2002).

Orthopyroxenes commonly contains thin lamellae of exsolved clinopyroxene. The inverse phenomenon occurs but is less common. Orthopyroxene also contains tiny inclusions of spinel. The cleavage in the pyroxenes from the sample 04OM63a1 and 04OM63a2 are clearly bent and sometimes the pyroxenes are fractured while olivines display undulose extinction (Figure 2). Within those fractures some neoblasts of clinopyroxene and orthopyroxene appear. This can be attributed to a deformation

process undergone by the samples within the upper mantle (e.g. Mercier and Nicolas, 1975).

The lherzolites have porphyroclastic or equigranular textures. Their modal compositions roughly range from 10 to 20% of clinopyroxene, 60 to 85% of olivine, 10 to 30% of orthopyroxene, and <10% of spinel. The olivine and pyroxenes porphyroclasts can reach 4mm in size while the neoblasts are typically less than 0.5 mm in size. Spinel size ranges from a few microns to 1 mm. The spinels are generally interstitial or in inclusion in olivine and clinopyroxene (Figure 2).

The harzburgites commonly display porphyroclastic or equigranular textures and more rarely a protogranular one. Their modal composition ranges from 55 to 70% of olivine, 30 to 40% of orthopyroxene, and close to 5% of clinopyroxene and spinel. The olivine and orthopyroxene porphyroclasts can reach 8 mm in size while the neoblasts are always < 0.5 mm in size. Clinopyroxene is interstitial and commonly less than 1-2 mm in size. Spinels commonly occur as tiny inclusions (<1 mm) in the silicates or as vermicular interstitial slightly bigger crystals (1-2 mm).

Mineral composition:

Olivine, Orthopyroxene and Spinel (Table 1)

Olivine is the dominant mineral phase in all samples. Olivines in harzburgites and lherzolites are very magnesian with their Mg-number ($100*Mg/Mg+Fe_{total}$) ranging from 89 to 91.2. Olivines of harzburgites are commonly more magnesian than those of lherzolites. Olivine has low CaO (<0.15 wt.%), MnO (< 0.25 wt.%) and Cr_2O_3 (< 0.07 wt.%) contents and NiO contents ranging from 0.25 to 0.54 wt. %.

Orthopyroxenes show the same compositional range as olivines with Mg-number ($100*Mg/Mg+Fe_{total}$) varying from 89.5 to 92. The Al_2O_3 content of

orthopyroxene ranges from 2 to 5.5 wt. % and TiO_2 content is always very low (<0.15 wt. %). The Cr_2O_3 and CaO content ranges from 0.3 to 0.75 wt. % and 0.7 to 1.2 wt. %, respectively. It has to be noticed that the lherzolite 04OM62b2 and the harzburgite 04OM64b1 display the more aluminous (5.5 wt %) and titaniferous (0.15 wt%) and the less aluminous (2 wt%), more chromiferous (0.75 wt%) and magnesian (Mg-number: 92) orthopyroxene, respectively.

Most spinels are relatively unzoned magnesian and aluminous chromites with Mg-number and Cr-number (100*Cr/Cr+Al) ranging from 70 to 80 and from 16 to 19.5, respectively. However, spinels of two samples are out of this Cr-number range. The harzburgite 04OM62b1 and the lherzolite 04OM62b2 respectively contain a more and a less chromiferous spinel (Cr# = 60 and 11.2), the former being also a little bit less magnesian (Mg# =64.4). In a Cr-number vs. Mg-number diagram (Figure 3), spinels plot in the field defined by spinels from the mantle peridotitic xenoliths from Spitsbergen, which is also a continental rifting area (Ionov et al., 2002). They are also similar to the spinels of the Oman mantle xenoliths studied by Nasir et al. (2006) but different from those of the mantle section of the Oman ophiolite (Figure 3).

Clinopyroxene :

Major elements (Table 1)

Clinopyroxenes are commonly diopsides but in samples 04OM62b1 and 04OM62b2 where they are Mg-augites. The clinopyroxene major element compositions highlight an evolution from fertile lherzolites (sample 04OM62b2: Mg#: 88.8 and Al_2O_3: 7.5 wt% to refractory harzburgites Mg#: 93.8 and Al_2O_3: 2.5 wt%). Cr_2O_3 and TiO_2 contents of most samples are relatively homogeneous, varying respectively from 0.3 to 1 wt% and from 0 to 0.2 wt%. However, the Cr_2O_3 content (up to 1.6 wt%) of the

clinopyroxenes from the harzburgite 04OM62b2 and the Ti_2O content of clinopyroxenes of the lherzolite 04OM62b2 (0.5 wt. %) are higher. Finally Na_2O content of clinopyroxenes of both types of peridotite ranges from 0.4 to 1.4 wt%. In Figure 4 the clinopyroxenes display a range of composition similar to that defined by the clinopyroxenes from mantle peridotitic xenoliths from Spitsbergen. The clinopyroxenes of harzburgites have the same Al_2O_3 contents than that of the clinopyroxenes from the mantle peridotites of the Oman ophiolite (Monnier et al., 2006) but have higher Na_2O contents and commonly lower Cr_2O_3 contents (Figure 4). Finally, the clinopyroxenes of the mantle xenoliths from Oman studied by Nasir et al. (2006) display intermediate compositions between those of the studied lherzolites and those of the studied harzburgites.

Trace elements

Trace element abundances of clinopyroxenes are given in Table 2. The REE contents of clinopyroxenes of most of the studied harzburgites and lherzolites are characterised by similar patterns evolving almost regularly from spoon-shaped patterns to LREE-enriched patterns characterised by an almost HREE-flat shape (La_N/Yb_N: 2.5-30; La_N/Sm_N: 3.2-24; Sm_N/Yb_N: 0.25-4.6; Ho_N/Lu_N : 0.88-1.15; Figure 5). These clinopyroxenes also display similar trace element patterns characterised by strong negative Ba, Nb, Zr, Hf and Ti anomalies. They appear to be similar to those of mantle peridotite xenoliths in alkaline lavas from Spitsbergen which have been subdivided into two types: the type-1 is characterized by spoon-shaped REE patterns and the type-2 displays LREE-enriched patterns (Ionov and al., 2002, Figure 5).

Only the lherzolite 04OM62b2 and the harzburgite 04OM62b1 display different REE patterns, being LREE-depleted (La_N/Yb_N: 0.29; La_N/Sm_N: 0.35; Sm_N/Yb_N: 0.82;

247 Ho_N/Lu_N: 1.16) and LREE-enriched with HREE fractionation (La_N/Yb_N: 9.32; La_N/Sm_N:
248 1.52; Sm_N/Yb_N: 6.14; Ho_N/Lu_N: 2.99), respectively (Figure 6). The clinopyroxene trace
249 element pattern of the lherzolite 04OM62b2 displays negative Nb and Ti anomalies
250 and a slight positive Sr anomaly while that of the harzburgite 04OM62b1 shows
251 negative Ba, Nb, Zr, Hf and Ti anomalies and a similar slight positive Sr anomaly
252 (Figure 6).
253

254 # Discussion

255

256 The studied suite of mantle xenoliths included in the alkaline lavas from the Al
257 Ashkharah region in Oman is composed lherzolites and harzburgites last equilibrated
258 within the mantle spinel peridotite stability field. We estimate their temperatures of
259 equilibration within the spinel stability field by using the geothermometers of Wells
260 (1977) and Brey and Kohler (1990), both based on the orthopyroxene/clinopyroxene
261 pair. Irrespective of the lithology (lherzolite and harzburgite), the temperature
262 estimates all range between 900 and 1150 °C using the calibration by Wells and
263 between 850 °C and 1160 °C (at P: 1.5 GPa) with that of Brey and Kohler.

264 The fact that we found only spinel harzburgites and lherzolites in the present
265 study appears to be a main difference with the study of Nasir et al. (2006), who
266 describe spinel wehrlites and dunites in their suite of mantle xenoliths from the Al
267 Ashkharah area and spinel wehrlites, lherzolites and dunites in their mantle xenolith
268 suite from Muscat area (Figure 1). In both cases the sample sizes are very small (≤
269 2cm in size) and therefore the modal estimates need to be taken with caution. Our
270 suite of samples is very close in terms of petrographic diversity to the mantle
271 xenoliths (harzburgites and lherzolites) from Spitsbergen (Ionov et al., 2002) as far as

peridotites are concerned. In the other hand they appear very different in term of petrographic diversity and mineral compositions from the mantle peridotites from the Oman ophiolite (mostly harzburgites and dunites in the ophiolite) (Figures 3, 4 and 8).

Most samples studied in the present study present several characteristics of solid residues resulting from partial melting, including high Mg number of olivine and pyroxenes, high Cr_2O_3 content of spinel. The HREE patterns of the clinopyroxenes are also in agreement with such a process (Figure 5). In order to estimate the degree of partial melting experienced by the Oman upper mantle we used two methods: (i) Firstly, we estimated the degree of partial melting by using the Cr# of spinel following the method of Hellebrand et al. (2001) calibrated for Cr# values in spinel ranging between 0.10 and 0.60, a range similar to that of our samples. The results mostly range from 2 to 8 % except for the harzburgites 04OM58b1 and 04OM62b1 that give estimates of 13 and 19 %, respectively. (ii) Secondly, we compared the REE contents of the clinopyroxenes with those computed using a model of fractional melting for a primitive spinel-peridotite mantle source, based on the method described by Johnson et al. (1990) (Figure 7). The starting composition and melting modes are those given by Hellebrand et al., (2002). In Figure 7 the REE from Dy to Yb are in good agreement with the partial melting model. The estimated degrees of melting using the HREE (Dy-Yb), which are the least subjected to metasomatism, range from 1 to about 6 % (Figure 7). This is with the exception of the harzburgite 04OM62b1, for which the partial melting modelling indicates inconsistent partial melting degrees between 10% (for Er) and 15% (for Yb). This is not plausible if we consider melting in the stability field of spinel because Er and Yb have very similar partition coefficients, such as in the present model. The MREE and HREE contents

297 of the clinopyroxene in harzburgite 04OM62b1 could also indicate that the
298 clinopyroxenes in this xenolith were in equilibrium with garnet because of the higher
299 partition coefficients for HREE in garnet. Moreover, the LREE and MREE from La to
300 Gd do not match the partial melting modelling. The clinopyroxenes have LREE and
301 MREE that are more enriched than predicted from the partial melting modelling.
302 These enrichments in LREE and MREE most probably reflect processes that
303 occurred after the partial melting event (see below). Finally in the harzburgite
304 04M62b1 the best estimate of the partial melting degree is given by the Cr# of spinel
305 using the method of Hellebrand et al. (2002), i.e. a degree close to 19%.

306 In the other hand, beside the evidence for partial melting processes (see
307 above) the majority of the studied Oman spinel peridotite xenoliths display evidence
308 for mantle metasomatism. This is supported by the concomitant increase of the Na
309 and Cr contents of clinopyroxenes (Figure 8). the REE patterns of most of the
310 clinopyroxenes (spoon-shaped and LREE-enriched) and the enrichment in the most
311 incompatible elements (Th, U, Sr), that point out to mantle metasomatism. The
312 selective enrichments in the most incompatible elements, LREE and MREE in mantle
313 clinopyroxenes are widely accepted to be the result of the infiltration of a fluid or of a
314 melt into the mantle rocks (e.g. O'Reilly and Griffin, 1988; Coltorti et al., 1999; Van
315 Achterberg et al., 2001; Grégoire et al., 2003 and 2005). The fact that only the most
316 incompatible trace elements (Th, U, Sr, LREE) are enriched in numerous samples is
317 in agreement with the percolation of a metasomatic agent at low melt/rock ratio. Thus
318 it appears that the studied mantle xenoliths from Oman record two types of
319 processes : partial melting and metasomatism.

320 Most of the clinopyroxenes from the mantle peridotites from the Al Ashkharah
321 area display REE patterns similar to those of the mantle spinel peridotite xenoliths

entrained by the alkaline lavas from Spitsbergen (Ionov et al., 2002 a and b; Figure 6). Ionov et al. (2002) proposed a two-stage evolution model to explain the history of xenoliths from Spitsbergen. First partial melting of a more or less fertile peridotitic mantle (degree of partial melting up to 22% for the most refractory samples), which formed residues characterized by LREE-depleted patterns. These melting residues were subsequently metasomatised by OIB-like carbonate-rich mafic silicate melts (Ionov et al., 2002 a and b). This metasomatic event led to the re-enrichment in the most incompatible elements and LREE (±MREE) in the clinopyroxenes such as in Figure 6. If we compare the Spitsbergen mantle clinopyroxenes with the studied Oman mantle clinopyroxenes, the later display very similar REE and incompatible trace element patterns (Figure 5) and therefore it is plausible that the metasomatic agents are similar in composition in the two cases. Finally the same two-stage evolution model can be invoked to explain the trace element compositions of most samples from this study. The studied mantle xenoliths from Al Ashkarah have been affected in a first stage by partial melting degrees between 1 to a maximum of 19 %. Later, in a second stage, the melting residues have suffered a metasomatic event leading to the re-enrichment in the most incompatible elements and LREE (±MREE) of the clinopyroxenes in the lherzolites, but also of the MREE ± HREE in the harzurgites, which are more sensitive to metasomatism. The metasomatic agent is probably a carbonate-rich mafic silicate melt enriched in highly incompatible trace elements and characterised by low abundances of Nb, Zr, Hf and Ti. Such characteristics allow to propose the hypothesis of a link between this metasomatic melt and the OIB-like tertiary alkaline melts of the same aera including the host lavas of mantle xenoliths studied by Worthing and Wilde (2002) and Nasir et al. (2006). This link is strengthened by the similarity of trace element patterns of the calculated

liquids in equilibrium with the clinopyroxenes of samples 04OM62b1 and OM63c1 with that of the host lava (Figure 9). For that calculation we used the clinopyroxene/basanite partition coefficients at 0.5 GPa from Adam and Green (2003). In such a model, the clinopyroxenes of samples 04OM62b2 (Lherzolite) and 04OM62b1 (Harzburgite) characterized by respectively a LREE-depleted REE pattern and a LREE-enriched one characterised by HREE fractionation may represent: (i) a witness of the first stage of the model (sample 04OM62b2), i.e. the process of partial melting or even the upper mantle before the partial melting as the clinopyroxene of this sample displays a REE pattern similar to that of the estimated primitive upper mantle (Figure 7) and (ii) a crystallization product of the metasomatic carbonate-rich silicate melt. Indeed the latter displays some similarities with the sample 4-90-1 from Ionov et al. (2002) which is a composite xenolith consisting of an amphibole-bearing wehrlite grading to an olivine-dominated zone with clusters of amphiboles. That sample is a fragment of a magmatic vein within the peridotitic mantle, a vein formed by a melt displaying similar REE content than that of the metasomatic agent responsible of the incompatible trace element enrichment of the Spitsbergen mantle xenoliths (Ionov et al., 2002).

Summary

The upper mantle equilibrated in the spinel stability field beneath the North West Al Ashkharah (East Oman) area mostly consists of lherzolites and harzburgites. This region of the upper mantle has been affected by two main petrogenetic processes: (i) an early partial melting event mostly of low degree leading to the formation of a LREE-depleted clinopyroxene in the peridotitic mantle residue and (ii) a metasomatic event linked to the circulation within this previously slightly depleted upper mantle of

a OIB-like carbonate-rich mafic silicate melt. The upper mantle beneath the North West Al Ashkharah therefore has a similar history than that of the upper mantle beneath Spitsbergen, an other continental rifting area. We tentatively suggest that the partial melting event is an old event while the metasomatic melt is related to the tertiary alkaline magmatic activity of the studied area related to the rifting of the Oman passive margin that lid to the opening of the Owen basin

ACKNOWLEDGMENTS

We warmly thank M. Monnereau for his help on the field and H. Al Azri from the Ministry of Commerce and Industry of Oman for constant support. Thin sections, electron microprobe analyses and ICP-MS analyses were performed using the facilities of the Observatoire Midi-Pyrénées, Paul Sabatier University, Toulouse. We are particularly indebted to F. de Parseval and J.-F. Mena for thin and thick section preparation, P. de Parseval for his help during microprobe data acquisition and F. Candaudap and R. Freydier for their help during LA-ICPMS data acquisition. This work was financially supported by the French Centre National de la Recherche Scientifique.

REFERENCES

Adam, J., Green, T., 2003. The influence of pressure, mineral composition and water on trace element partitioning clinopyroxene, amphibole and basanitic melts. European Journal of Mineralogy 15, 831-841.

Brey, G.P., Kohler, T., 1990. Geothermobarometry in four-phase lherzolites II. New thermobarometers, and practical assessment of existing thermobarometers. Journal of Petrology 31, 1353-1378.

Carpenter, R.L., Edgar, A.D, Thibault. 2002. Origine of spongy textures in clinopyroxene and spinel from mantle xenoliths, Hessian Depression, Germany. Mineralogy and Petrology 74: 149-162.

Coleman, R.G., 1981. Tectonic setting for ophiolite obduction in Oman. Journal of Geophysical Research 86, 2497-2508.

Coltorti, M., Bonadiman, C., Hinton, R.W., Siena, F., Upton, B.G.J., 1999. Carbonatite metasomatism of the oceanic upper mantle: evidence from clinopyroxenes and glasses in ultramafic xenoliths of Grande Comore, Indian Ocean. Journal of Petrology 40, 133-165.

Dantas, C., Ceuleneer, G., Grégoire, M., Python, M., Freydier, R., Warren, J., Dick H.B.J., 2007. Pyroxenites dredged along the south-west Indian Ridge, 9°-16°E: cumulates from incremental melt fractions produced at top of a cold melting regime. Journal of Petrology 48, 647-660.

Delpech, G., Grégoire, M., O'Reilly, S.Y., Cottin, J.Y., Moine, B.N., Michon, G. 2004. Feldspar from carbonate-rich metasomatism in the oceanic mantle under Kerguelen Islands (South Indian Ocean), Lithos 75, 209-237.

Fournier, M., Chamot-Rooke, N., Petit, C., Fabbri, O., Huchon, P., Maillot, B., Lepvrier C., 2008. In situ evidence for dextral active motion at the Arabia-India plate boundary. Nature Geosciences 1, 54-58.

Glennie, K.W., Boeuf, M.G.A., Hughes-Clark, M.W., Moody-Stuart, M., Pilaar, W.F.H., Reinhardt, B.M., 1974. Geology of the Oman mountains. Verhandling Koninkelijk Nederlands Geologisch Mijnboukundig Genootschap 31, 423 pp.

Gnos, E., Immenhauser, A., Peters T., 1997. Late Cretaceaous/Early Tertiary convergence between the Indian and Arabian plates recorded in ophiolites and related sediments. Tectonophysics 271, 1-19.

Gnos, E., Perrin, M., 1995. Formation and evolution of the Masirah ophiolite constrained by paleomagnetic study of volcanic rocks. Tectonophysics 253, 53-64.

Gnos, E., Peters, T., 2003. Mantle xenolith-bearing Maastrichtian to Tertiary alkaline magmatism in Oman. Geochemistry, Geophysics, Geosystems (G-cubed) 4, 8620, doi: 10.1029/2001GC000229.

Grégoire, M., Lorand, J.P., Cottin, J.Y., Giret, A., Mattielli, N., Weis, D., 1997. Petrology of Kerguelen mantle xenoliths: Evidence of a refractory oceanic mantle percolated by basaltic melts beneath the Kerguelen archipelago. European Journal of Mineralogy 9, 1085-1100.

Grégoire, M., Moine, B.N., O'Reilly, S.Y., Cottin, J.Y., Giret, A., 2000. Trace element residence and partitioning in mantle xenoliths metasomatized by highly alkaline, silicate- and carbonate-rich melts Kerguelen Islands, Indian Ocean. Journal of Petrology 41, 477-509.

Grégoire, M., Bell, D.R., Le Roex, A.P., 2003. Garnet lherzolites from the Kaapvaal craton South Africa: trace elements evidence for a metasomatic history. Journal of Petrology 44, 629-657.

Grégoire, M., Tinguely, C., Bell, D.R, Le Roex, A.P., 2005. Spinel lherzolite xenoliths from the Premier kimberlite (Kaapvaal craton, South Africa): Nature and evolution of the shallow upper mantle beneath the Bushveld complex. Lithos 84, 185-205.

Grégoire, M., Chevet, J., Maaloe, S. Composite xenoliths from Spitsbergen: evidence of the circulation of MORB-related melts within the upper mantle. Submitted to Geological Society of London special publication.

464 Hellebrand, E., Snow, J.E., Dick, H.J.B., Hofmann, A., 2001. Coupled major and
465 trace elements as indicators of the extent of melting in mid-ocean-ridge peridotites.
466 Nature 410, 677-681.
467
468 Hellebrand, E., Snow, J.E., Hoppe, P., Hofmann, A., 2002. Garnet-field melting and
469 late-stage refertilization in “residual” abyssal peridotites from the Central Indian
470 Ridge. Journal of Petrology 43, 12, 2305-2338.
471
472 Ionov, D. A., Bodinier, J. L., Mukasa, S. B., Zanetti, A., 2002a. Mechanisms and
473 sources of mantle metasomatism: major and trace element compositions of peridotite
474 xenoliths from Spitsbergen in the context of Numerical Modelling. Journal of
475 Petrology 43, 2219-2259.
476
477 Ionov, D. A., Mukasa, S. B., Bodinier, J. L., 2002b. Sr-Nd-Pb isotopic compositions.
478 of peridotite xenoliths from Spitsbergen. Numerical Modelling indicates Sr-Nd
479 decoupling in the mantle by melt percolation processes. Journal of Petrology 43,
480 2261-2278.
481
482 Johnson, K.T. M., Dick, H. J. B., Shimizu, N., 1990. Melting in the oceanic upper
483 mantle: an ion microprobe study of diopsides in abyssal peridotites. Journal of
484 Geophysical Research 95, 2661-2678.
485
486 Lenoir, X., Garrido, C.J., Bodinier, J.-L., Dautria, J.-M., 2000. Contrasting lithospheric
487 mantle domains beneath the Massif Central (France) revealed by geochemistry of
488 peridotite xenoliths. Earth and Planetary Science Letters 181, 359-375.
489
490 McDonough, W. F., Sun, S., 1995. The composition of the Earth. Chemical Geology
491 120, 223-253.
492
493 Mercier, J-C. C., Nicolas, A., 1975. Textures and fabrics of upper-mantle peridotites
494 as illustrated by xenoliths from basalts. Journal of Petrology 16, 454-487.
495

Monnier, C., Girardeau, J., Le Mée, L., Polvé, M. 2006. Along-ridge petrological segmentation of the mantle in the Oman ophiolite. Geochemistry, Geophysics, Geosystems (G-cubed) 7, Q11008, doi: 10.1029/2006GC001320.

Moseley, F., 1969.The upper cretaceous ophiolite complex of Masirah island, Oman. Geological Journal, 6, 293-306.

Nasir, S., Al-Sayigh, A., Alharthy, A., Al-Lazki, A., 2006. Geochemistry and petrology of Tertiary volcanic rocks and related ultramafic xenoliths from the central and eastern Oman Mountains. Lithos 90, 249–270

O'Reilly, S.Y., Griffin, W.L., 1988. Mantle metasomatism beneath Victoria, Australia I: metasomatic processes in Cr-diopside lherzolites. Geochimica et Cosmochimica Acta 52, 433– 447.

Patriat, P., Achache, J., 1984. India-Eurasia collision chronology has implications for crustal shortening and driving mechanisms of plates. Nature 311, 615-621.

Peters, T., Mercolli, I., 1998. Extremely thin oceanic crust in the Proto-Indian Ocean: evidence from the Masirah ophiolite, Sultanate of Oman. Journal of Geophysical Research 103, 677-689.

Platel, J.-P., Roger, J., 1989. Evolution géodynamique du Dhofar (Sultanat d'Oman) pendant le Crétacé et le Tertiaire en relation avec l'ouverture du golfe d'Aden. Bulletin de la Société Géologique de France 8, 253-263.

Pouchou, J., Pichoir, J., 1984. "PAP" Z procedure for improved quantitative microanalysis. Microanalysis, 104-106.

Royer, J.-Y., Chaubey, A.K., Dyment, J., Bhattacharya, G.C., Srinivas, K., Yatheesh, V., Ramprasad, T., 2002. Paleogene plate tectonic evolution of the Arabian and Eastern Somali basins. In: Clift, P.D., Kroon, D., Gaedicke, C., Craig, L. (eds). *The tectonic and climatic evolution of the Arabian Sea region*. Geological Society of London Special Publications 195, 7-23.

Van Achterbergh, E., Griffin, W.L., Stiefenhofer, J., 2001. Metasomatism in mantle xenoliths from the Letlhakane kimberlites: estimation of element fluxes. Contributions to Mineralogy and Petrology 141, 397-414.

Wells, P.R.A., 1977. Pyroxene thermometry in sample and complex system. Contributions to Mineralogy and Petrology 62,129-139.

Witt-Eickschen, G., Seck, H.A., Mezger, K., Eggins, S.M., Altherr, R., 2003. Lithospheric mantle evolution beneath the Eifel (Germany): 709 constraints from Sr–Nd–Pb isotopes and trace element abundances 710 in spinel peridotite and pyroxenite xenoliths. Journal of Petrology 44, 1077–1095.

Worthing, M.A., Wilde, A.R., 2002. Basanites related to Eocene extension from NE Oman. Journal Geological Society of London 159, 469-483.

TABLE CAPTIONS

Table 1. Major (EMPA; wt %) element concentrations for Oman lherzolites and harzburgites olivines, orthopyroxenes, spinels and clinopyroxenes. Mg#= Mg/(Mg $+Fe_{Total}$) x100.

Table 2. Average REE and trace (LA-ICP-MS; ppm) element concentrations for clinopyroxenes of Oman mantle xenoliths. (n= number of analysis).

FIGURE CAPTIONS

Figure 1: Location map of the studied area (after Gnos and Peters, 2003)

559 Figure 2: Microphotographs. A: An angular-shaped protogranular harzburgite xenolith
560 (size of the xenolith: 13 mm x 6 mm); B: porphyroclastic lherzolite, field of view: ~ 6
561 mm.
562
563 Figure 3: Diagram Cr# (100xCr/Cr+Al) versus Mg# (100xMg/Mg+Fe_{total}) of spinels of
564 mantle xenoliths from the North West Al Ashkharah (East Oman) area. Double
565 crosses: Harzburgites; Crosses: Lherzolites; Filled diamonds: Spitsbergen mantle
566 lherzolite and harzburgite xenoliths from Ionov et al. (2002); Filled squares in a dark
567 grey field: mantle peridotite xenoliths from Oman (Nasir et al., 2006); Empty squares
568 in a ligth grey field: mantle peridotites from Oman ophiolite from Monnier et al.
569 (2006).
570
571 Figure 4: Diagrams Al_2O_3, Cr_2O_3 and Na_2O versus Mg# (100xMg/Mg+Fe_{total}) of
572 clinopyroxenes of mantle xenoliths from the North West Al Ashkharah (East Oman)
573 area. Same legend as Figure 3.
574
575 Figure 5: Primitive mantle-normalized REE and incompatible trace element patterns
576 of the clinopyroxenes characterised by spoon-shaped REE or LREE-enriched
577 patterns (this study) and from Ionov et al. (2002). See text for explanation.
578 Normalization values are from McDonough and Sun (1995).
579
580 Figure 6: Primitive mantle-normalized trace element patterns of the clinopyroxenes
581 from the harzburgite 04OM62B1 and the lherzolite 04OM62B2 (this study) and of the
582 sample 4-90-1 from Spitsbergen (Ionov et al., 2002). See text for explanation.
583 Normalization values are from McDonough and Sun (1995).

584

585 Figure 7: Non-modal partial melting modelling for the REE in clinopyroxenes from the
586 North West Al Ashkharah. The data are normalised to the CI-Chondrite of
587 McDonough and Sun (1995). Most clinopyroxenes display HREE contents that are in
588 agreement with a partial melting degree of ~1 to 5%, except for the harzburgite
589 04OM62b1, for which the HREE cannot be accounted for by a single stage history.

590

591 Figure 8: Diagram Cr_2O_3 versus Na_2O of clinopyroxenes of mantle xenoliths from the
592 North West Al Ashkharah (East Oman) area. Same legend as Figure 3.

593

594 Figure 9: Hypothetical melts in equilibrium with clinopyroxene from metasomatised
595 harzburgites 04OM62b1 and 04OM63c1 compared to the host basanite (Nasir et al.,
596 2006). Normalising values from McDonough and Sun (1995) and Cpx/basanite
597 partition coefficients at 0.5 GPa from Adam and Green (2003).

598

599

Figure 1

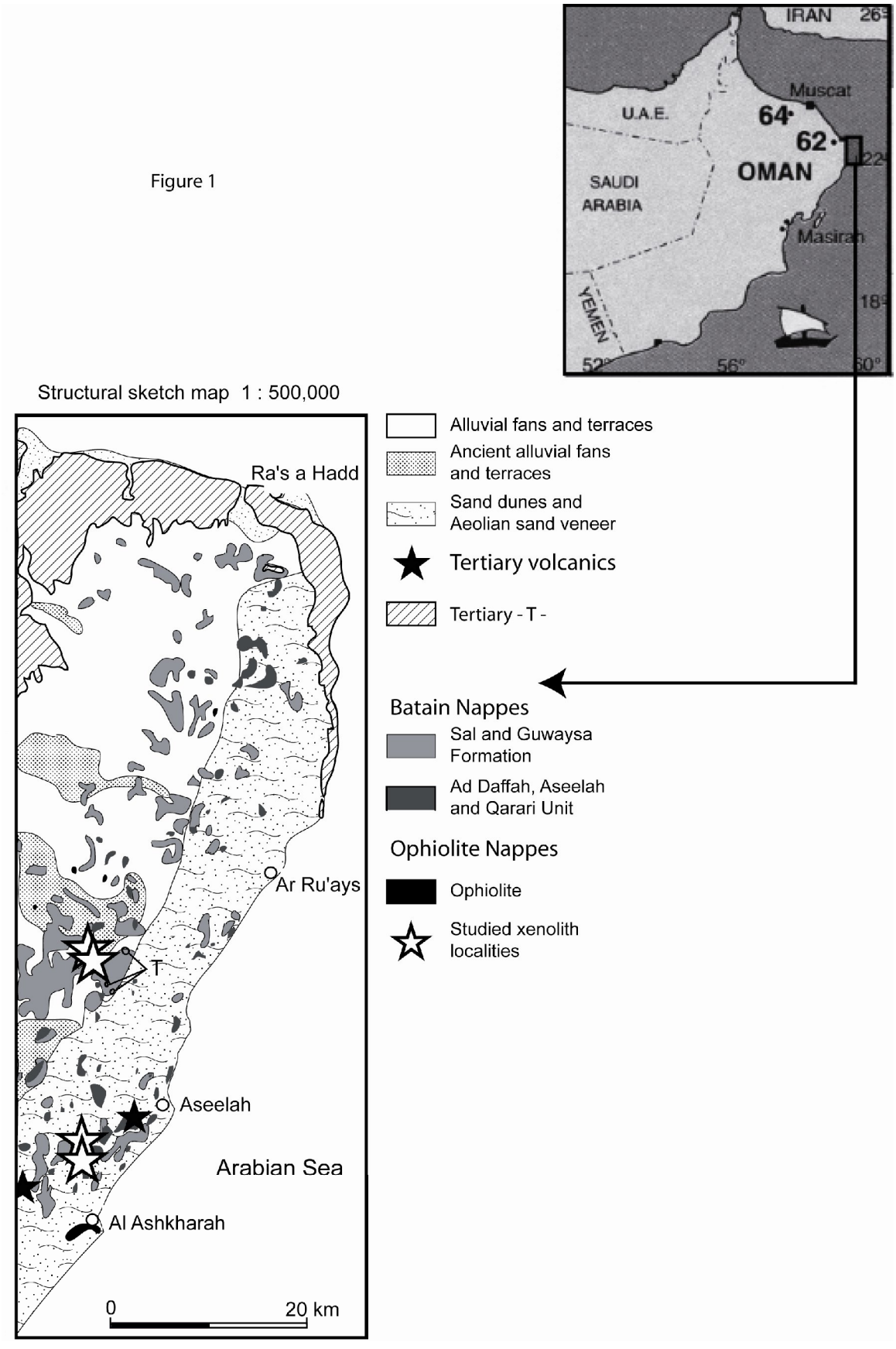
Figure 1
IRAN
Muscat
U.A.E.
64
62
OMAN
SAUDI ARABIA
Masirah
YEMEN
Structural sketch map 1 : 500,000
Ra's a Hadd
Ar Ru'ays
T
Aseelah
Arabian Sea
Al Ashkharah
0
20 km
Alluvial fans and terraces
Ancient alluvial fans and terraces
Sand dunes and Aeolian sand veneer
Tertiary volcanics
Tertiary - T -
Batain Nappes
Sal and Guwaysa Formation
Ad Daffah, Aseelah and Qarari Unit
Ophiolite Nappes
Ophiolite
Studied xenolith localities

Figure 2

Figure 2

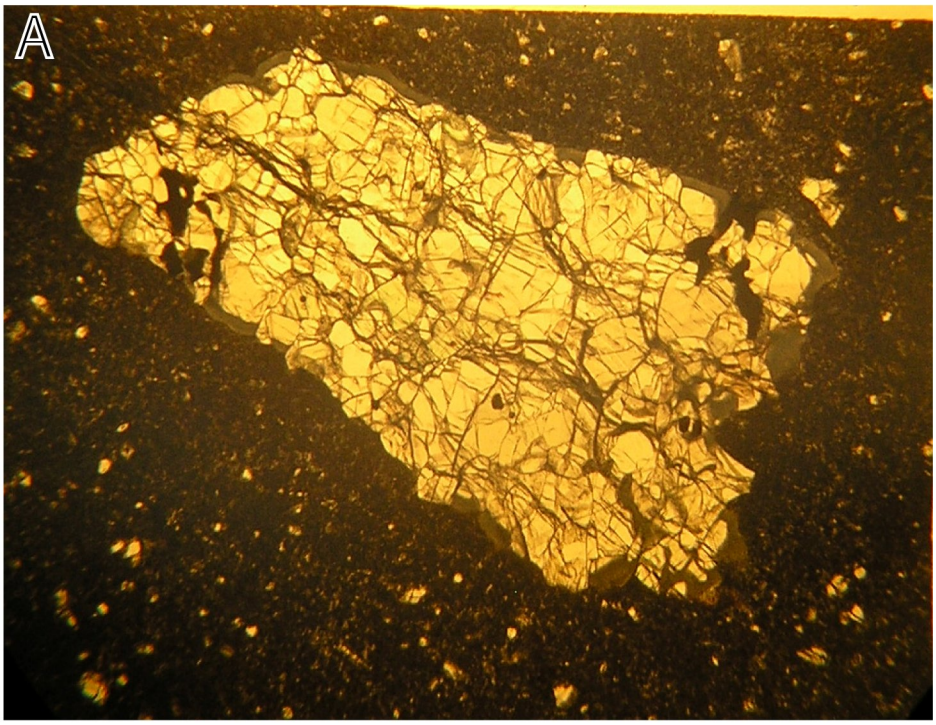

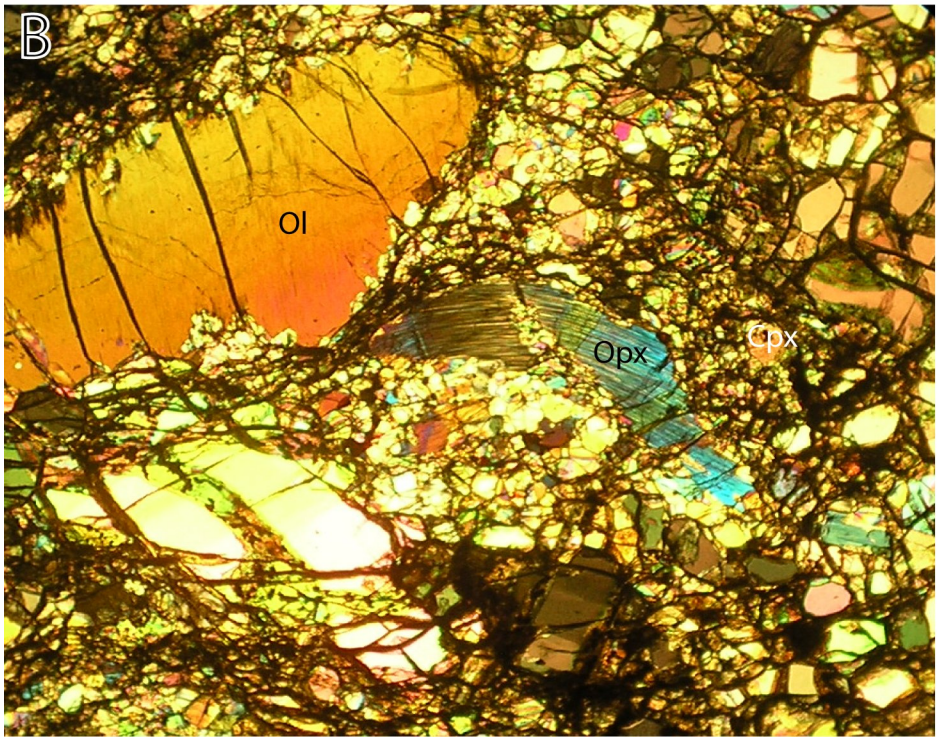

Figure 3

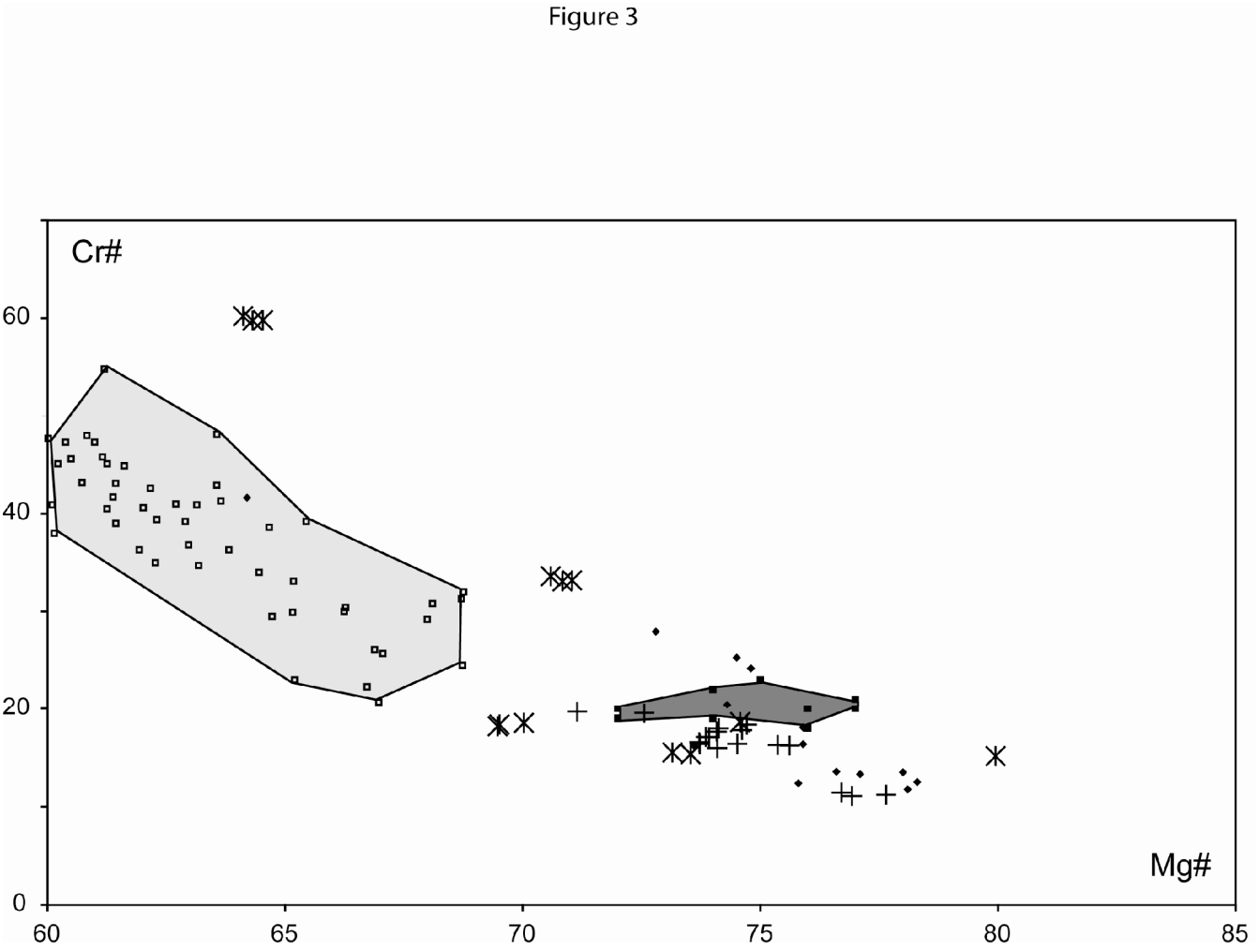

Figure 4

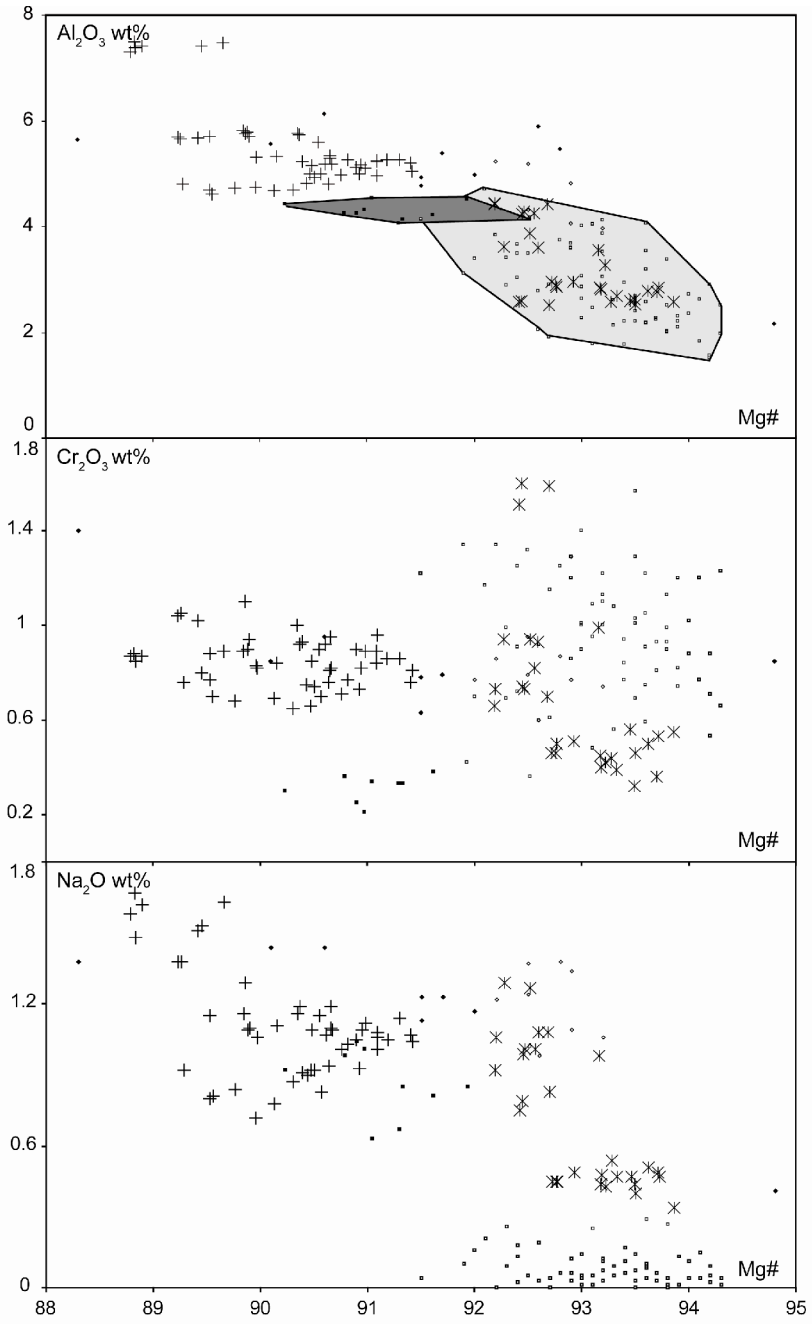

Figure 4

Figure 5

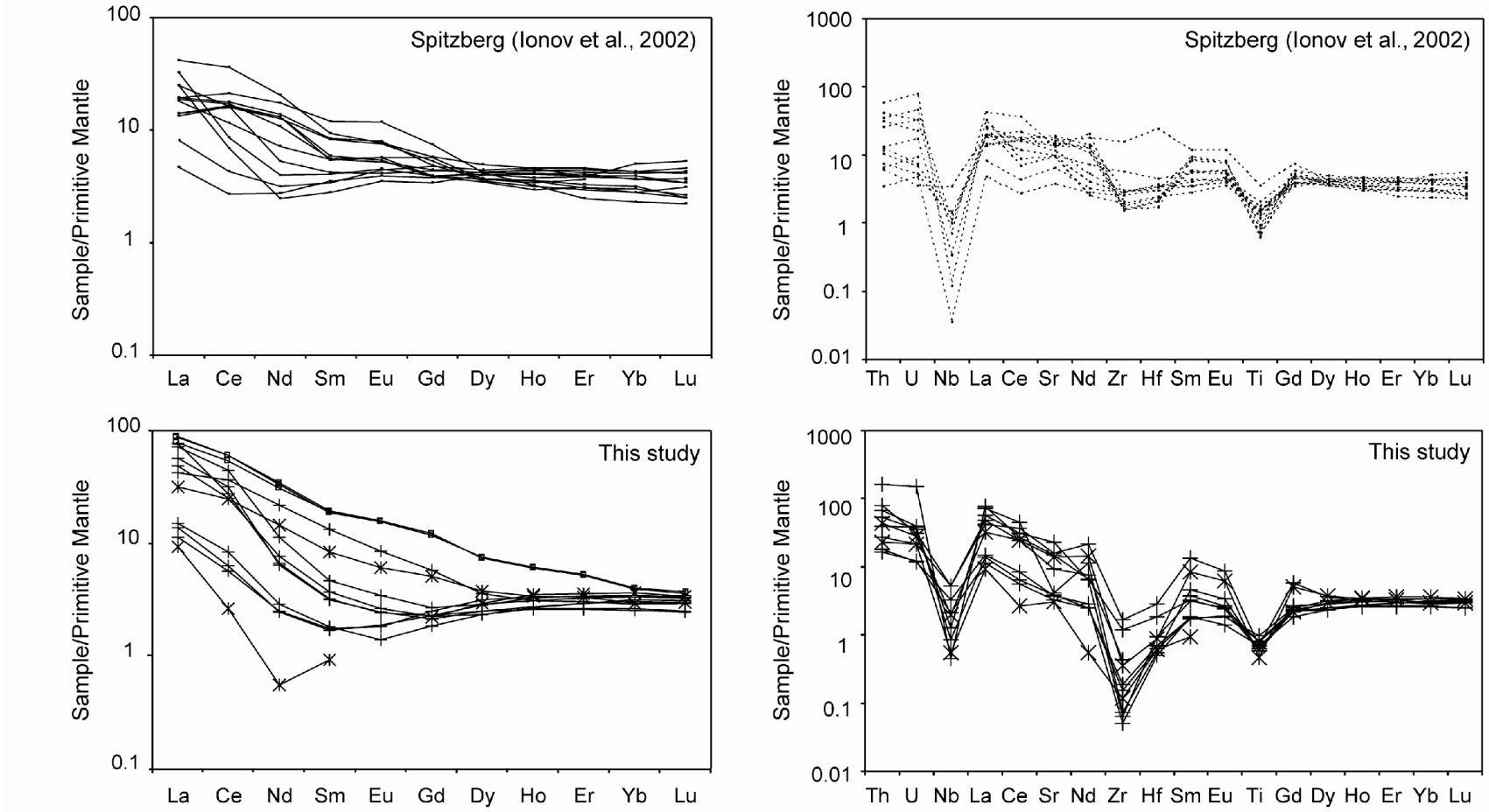
Figure 5
Spitzberg (Ionov et al., 2002)
Sample/Primitive Mantle
100
10
1
0.1
La Ce Nd Sm Eu Gd Dy Ho Er Yb Lu
Spitzberg (Ionov et al., 2002)
Sample/Primitive Mantle
1000
100
10
1
0.1
0.01
Th U Nb La Ce Sr Nd Zr Hf Sm Eu Ti Gd Dy Ho Er Yb Lu
This study
Sample/Primitive Mantle
100
10
1
0.1
La Ce Nd Sm Eu Gd Dy Ho Er Yb Lu
This study
Sample/Primitive Mantle
1000
100
10
1
0.1
0.01
Th U Nb La Ce Sr Nd Zr Hf Sm Eu Ti Gd Dy Ho Er Yb Lu

Figure 6

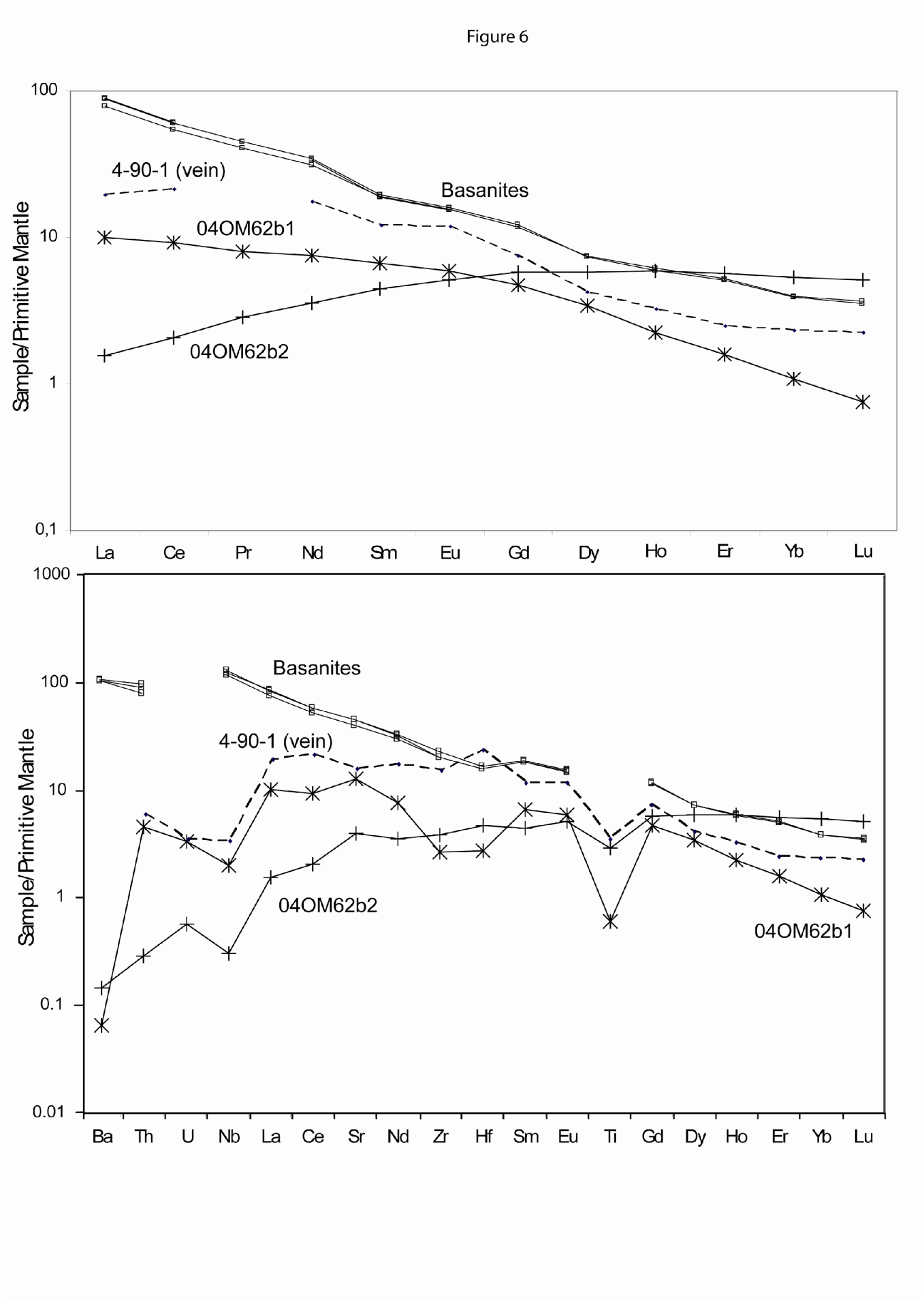
Figure 6
100
10
1
0,1
Sample/Primitive Mantle
4-90-1 (vein)
Basanites
04OM62b1
04OM62b2
La
Ce
Pr
Nd
Sm
Eu
Gd
Dy
Ho
Er
Yb
Lu
1000
100
10
1
0.1
0.01
Sample/Primitive Mantle
Basanites
4-90-1 (vein)
04OM62b2
04OM62b1
Ba
Th
U
Nb
La
Ce
Sr
Nd
Zr
Hf
Sm
Eu
Ti
Gd
Dy
Ho
Er
Yb
Lu

Figure 7

Figure 7

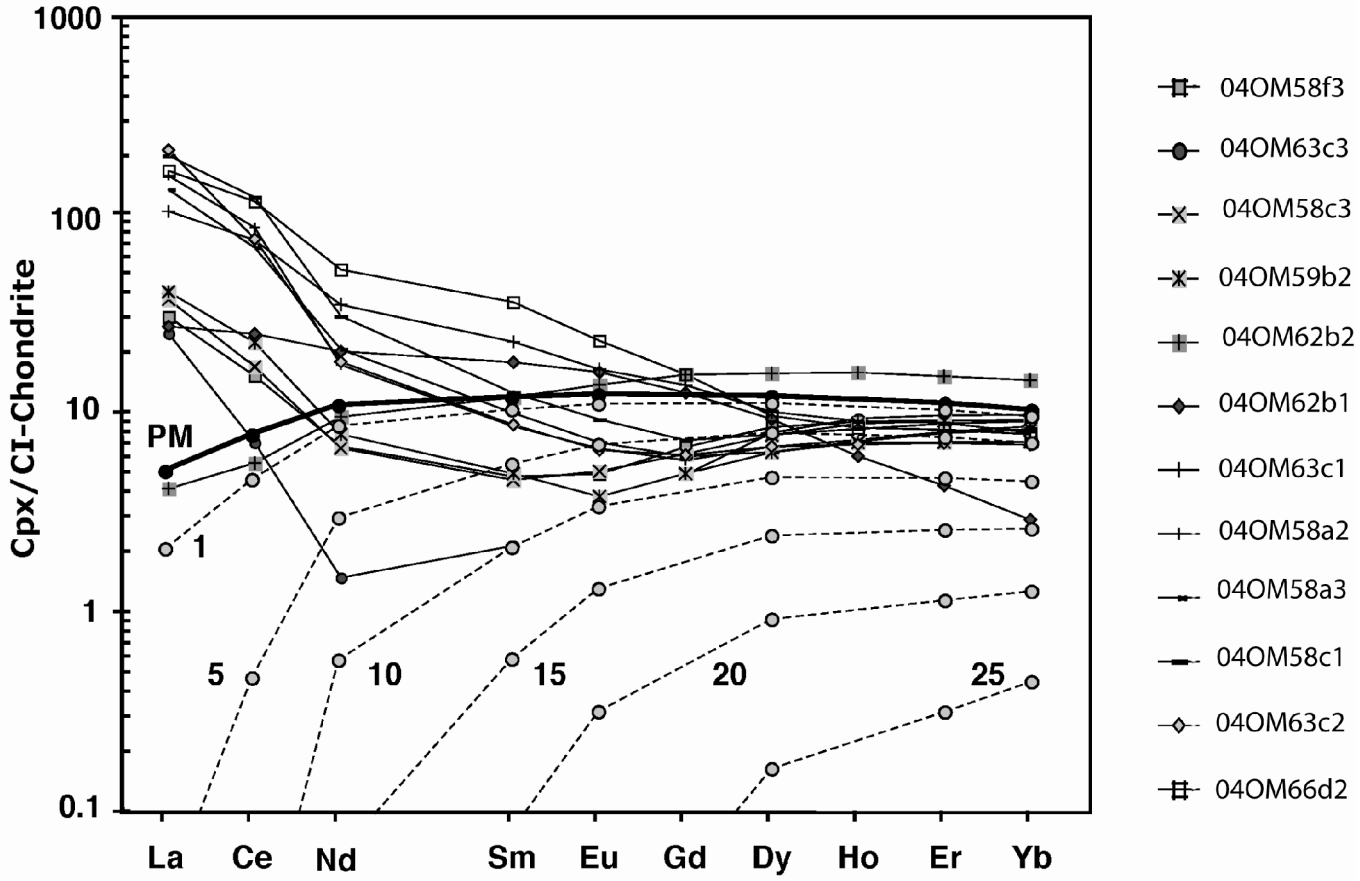

Figure 8

Figure 8

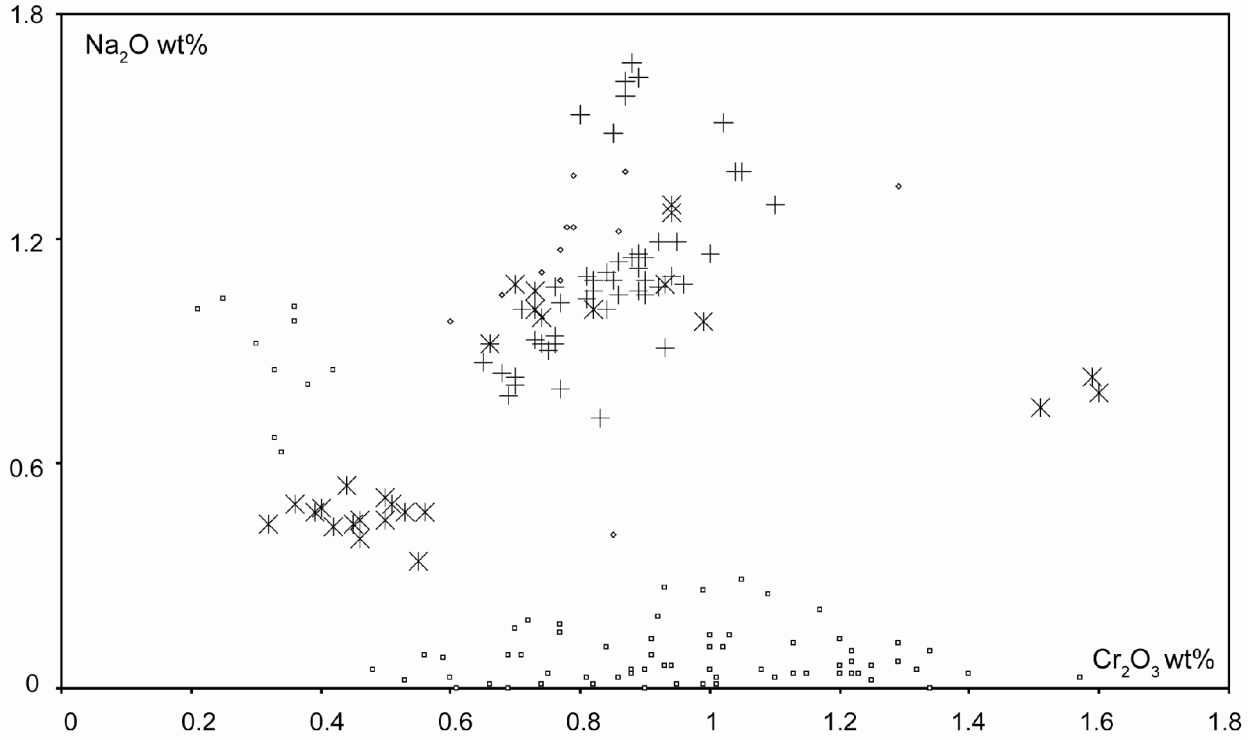

Figure 9

Figure 9

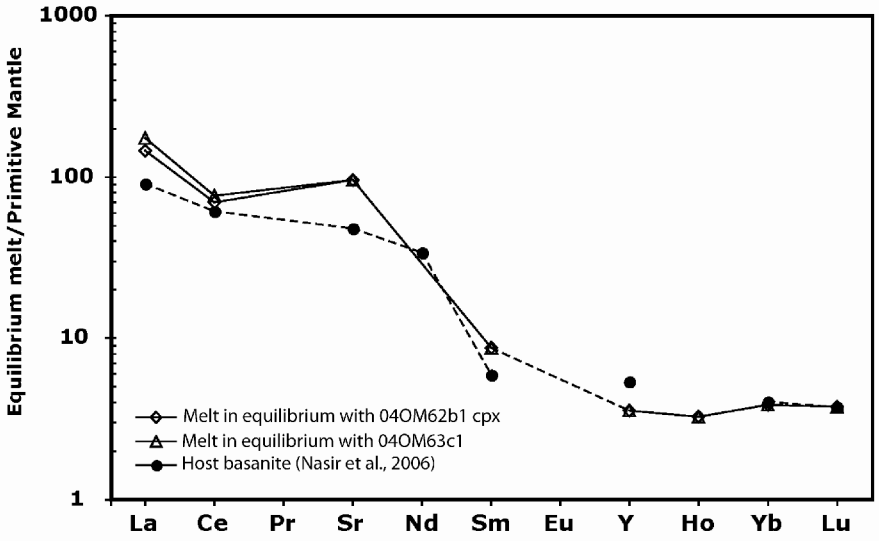

Table 1

Click here to download Table: Table 1.xls

	Harzburgites														**Lherzolites**																					
Olivine	04OM58b1	04OM58b1	04OM58b1	04OM63a2	04OM63a2	04OM63a2	04OM63c1	04OM63c3	04OM63c3	04OM63c3					04OM58a2	04OM58a2	04OM58a2	04OM58a2	04OM58a2	04OM58a2	04OM58a2	04OM58a3	04OM58a3	04OM58c3	04OM58c3	04OM58f3	04OM58f3	04OM58f3	04OM59b2	04OM62b2	04OM62b2	04OM62b2	04OM63c2	04OM66d2	04OM66d2	04OM66d2
SiO2	40.93	41.43	41.82	41.34	41.08	40.50	41.31	41.47	41.38	41.11					40.54	40.85	40.55	40.6	41.08	40.89	41.11	40.91	40.55	41.77	41.45	41.31	41.44	41.19	41.28	41.36	40.79	41.3	40.88	41.06	40.85	40.73
Cr2O3	-	0.01	0.05	0.01	0.01	0.04	0.04	0.02	-	0.04					0.01	-	0.03	-	-	0.01	0.02	0.02	0.10	-	0.02	-	0.05	0.03	0.03	0.04	0.03	0.03	-	0.06	0.03	-
FeO	8.81	8.66	8.62	9.44	9.25	8.89	9.39	8.70	8.91	9.11					9.54	9.63	9.42	9.02	9.53	9.15	9.39	10.16	9.38	8.97	9.53	9.28	9.36	9.21	9.60	9.76	9.88	9.72	9.98	10.70	9.56	10.64
MnO	0.22	0.21	0.10	0.15	0.07	0.11	0.20	0.09	0.07	0.09					0.12	0.11	0.18	0.12	0.05	0.21	0.20	0.09	0.14	0.14	0.08	0.19	0.10	0.10	0.13	0.08	0.10	0.10	0.14	0.22	0.20	0.13
MgO	49.46	49.81	49.82	49.56	49.47	49.6	49.48	49.11	49.79	49.12					49.13	49.47	49.34	49.29	49.09	49.52	49.42	49.13	48.75	49.63	48.89	49.64	49.19	49.18	48.63	48.75	48.85	48.25	48.81	48.49	49.42	48.77
CaO	0.06	0.02	0.12	0.05	0.03	0.08	0.05	0.04	0.06	-					0.13	0.06	0.04	0.08	0.07	0.04	0.04	0.06	0.08	0.10	0.05	0.08	0.06	0.09	0.05	0.11	0.07	0.07	0.05	0.22	0.06	0.11
NiO	0.37	0.36	0.42	0.34	0.47	0.40	0.33	0.44	0.35	0.32					0.34	0.49	0.33	0.36	0.37	0.37	0.42	0.25	0.36	0.37	0.46	0.43	0.39	0.36	0.38	0.41	0.35	0.30	0.47	0.41	0.47	0.38
Total	99.84	100.50	100.96	100.89	100.38	99.62	100.80	99.87	100.56	99.80					99.83	100.61	99.88	99.47	100.19	100.19	100.59	100.61	99.37	100.97	100.48	100.93	100.59	100.16	100.10	100.51	100.08	99.76	100.35	101.16	100.59	100.76
Mg#	90.91	91.11	91.15	90.34	90.50	90.86	90.37	90.96	90.87	90.57					90.17	90.15	90.32	90.69	90.17	90.60	90.36	89.60	90.25	90.79	90.14	90.50	90.35	90.49	90.03	89.90	89.81	89.84	89.71	88.98	90.21	89.09
	Harzburgites														**Lherzolites**																					
Orthopyroxene	04OM58b1	04OM63a2	04OM63a2	04OM63a2	04OM63a2	04OM63a1	04OM63a1	04OM63a1	04OM63a1	04OM63c3	04OM63c3	04OM63c1	04OM62b1	04OM62b1	OM66d2	04OM58f3	04OM63c2	04OM62b2	04OM59b2	04OM59b2	04OM58a2	04OM58a2	04OM58a2	04OM58a2	04OM58a3	04OM58a3	04OM58a3	04OM58a3	04OM58a3	04OM58a3	04OM58c3					
SiO2	56.75	56.13	56.29	56.15	56.77	56.1	56.73	56.46	56.99	55.86	55.44	56.97	57.25	57.07	55.13	54.88	55.78	54.19	55.4	55.57	54.91	55.18	54.62	54.59	54.87	54.59	55.12	54.62	54.64	54.82	55.7					
TiO2	-	-	-	-	-	0.01	-	-	0.02	0.03	0.04	0.01	0.04	-	0.04	0.06	-	0.15	0.02	0.01	0.02	-	0.06	-	-	-	-	-	0.03	0.01	0.05					
Al2O3	2.61	2.72	2.73	3.10	2.89	2.95	2.70	2.66	2.51	3.05	3.21	2.71	2.03	1.87	4.25	4.16	3.88	5.61	4.36	4.21	4.33	4.11	3.97	4.13	4.76	4.53	4.59	4.57	4.70	4.66	4.13					
Cr2O3	0.54	0.32	0.31	0.35	0.28	0.37	0.32	0.30	0.31	0.43	0.30	0.41	0.76	0.77	0.51	0.55	0.43	0.47	0.52	0.47	0.51	0.38	0.40	0.45	0.54	0.52	0.47	0.57	0.58	0.48	0.53					
FeOtotal	5.54	5.71	5.85	5.85	5.87	6.00	6.04	5.60	5.70	5.53	5.71	5.93	5.13	5.20	6.24	5.65	6.84	6.18	6.38	6.04	5.93	6.22	6.25	6.06	6.12	6.41	6.23	6.31	6.05	6.22	6.00					
MnO	0.15	0.14	0.18	0.14	0.19	0.12	0.05	0.09	0.14	0.17	0.15	0.12	0.04	0.24	0.18	0.10	0.08	0.21	0.21	0.14	0.15	0.20	0.17	0.12	0.17	0.10	0.15	0.15	0.17	0.19	0.15					
MgO	33.83	34.12	33.98	33.64	34.23	33.76	33.89	33.91	33.92	33.28	33.65	33.59	33.82	33.51	32.90	32.93	32.39	31.77	32.90	32.67	32.73	33.14	32.87	32.79	32.54	32.53	32.68	32.41	32.36	32.43	32.89					
CaO	0.65	0.50	0.47	0.55	0.49	0.46	0.52	0.51	0.49	0.62	0.60	0.63	1.19	1.15	0.90	0.84	0.75	1.12	0.85	0.81	0.77	0.83	0.84	0.81	0.91	0.94	0.94	0.98	0.89	0.97	0.83					
Total	100.08	99.66	99.85	99.77	100.73	99.77	100.26	99.54	100.09	98.97	99.18	100.38	100.33	99.82	100.18	99.19	100.19	99.7	100.65	99.92	99.35	100.12	99.26	98.99	99.90	99.67	100.19	99.63	99.44	99.80	100.28					
Mg#	91.58	91.42	91.19	91.11	91.22	90.93	90.91	91.52	91.38	91.47	91.30	90.98	92.15	91.99	90.38	91.22	89.40	90.16	90.18	90.60	90.77	90.47	90.36	90.61	90.45	90.04	90.33	90.15	90.50	90.28	90.71					
Spinel	**Harzburgites**														**Lherzolites**																					
Label	04OM63a2	04OM63c2	04OM63c2	04OM63c2	04OM63a1	04OM58b1	04OM58b1	04OM58b1	04OM66c2	04OM66c22	04OM62b1	04OM62b1	04OM62b1		04OM62b21	04OM62b22	04OM62b2	OM66d2	OM66d2	04OM58f3	04OM58f3	04OM58f3	04OM59b2	04OM59b22	04OM58c3	04OM58a2	04OM58a2	04OM58a2	04OM58a3	04OM58a3	04OM58a3					
SiO2	0.01	0.08	0.01	0.04	0.09	0.07	0.08	0.04	0.07	0.02	0.02	0.07	0.07		0.07	0.05	0.10	0.06	0.08	0.08	0.08	0.07	0.05	0.04	0.06	0.07	0.09	0.09	0.06	0.09	0.04					
TiO2	-	0.09	0.05	0.01	-	0.10	0.09	0.06	0.13	0.15	0.29	0.30	0.25		0.20	0.14	0.22	0.03	0.04	0.03	0.05	0.03	0.05	0.04	0.05	-	0.03	0.03	0.01	0.05	-					
Al2O3	50.54	48.19	48.34	48.55	53.04	39.10	38.64	39.14	51.86	51.98	21.12	21.19	21.51		56.1	56.01	56.02	48.47	49.10	50.29	50.47	50.18	51.81	52.03	50.29	51.32	50.97	51.88	50.84	51.28	51.07					
Cr2O3	17.22	16.15	16.01	16.46	14.11	28.95	29.16	28.83	14.01	14.22	47.62	46.96	47.59		10.44	10.55	10.78	17.71	17.78	16.23	16.49	16.02	15.15	14.73	16.85	14.87	14.89	14.97	15.63	15.17	15.67					
FeOt	11.46	14.31	14.54	14.25	9.59	12.31	12.70	12.50	12.41	12.72	14.86	14.51	14.82		11.00	10.62	11.03	13.58	12.77	11.56	12.04	12.10	11.62	11.88	11.71	11.67	12.12	11.37	12.05	12.33	12.07					
MnO	0.14	0.17	0.12	0.17	0.08	0.17	0.12	0.15	0.11	0.17	0.22	0.07	0.22		0.07	0.15	0.08	0.07	0.16	0.15	0.08	0.09	0.06	0.05	0.17	0.11	0.02	0.12	0.08	0.17	0.11					
MgO	19.00	18.44	18.70	18.82	21.61	17.07	17.23	17.16	19.49	19.58	15.01	14.92	15.1		20.74	20.85	20.53	18.92	19.08	19.21	19.50	19.55	19.20	19.21	19.56	20.17	19.22	19.92	19.23	19.55	19.34					
ZnO	0.10	0.06	0.05	0.09	0.11	0.17	0.20	0.12	0.06	0.03	0.05	0.19	0.23		0.24	0.10	0.03	0.24	0.16	0.21	-	0.14	0.01	0.20	0.16	0.09	0.04	0.09	0.13	0.15	0.03					
NiO	0.36	0.20	0.37	0.50	0.32	0.27	0.21	0.26	0.44	0.36	0.24	0.18	0.11		0.31	0.33	0.33	0.34	0.43	0.28	0.27	0.32	0.45	0.40	0.40	0.49	0.42	0.42	0.29	0.28	0.43					
Total	98.98	98.1	98.67	99.38	99.26	98.34	98.60	98.43	98.89	99.57	99.73	98.66	100.21		99.44	99.06	99.33	99.80	99.91	98.29	99.23	98.82	98.56	98.80	99.50	99.14	98.06	99.17	98.58	99.38	99.03					
Mg#	74.57	69.51	69.47	70.03	79.95	71.04	70.59	70.84	73.53	73.15	64.12	64.53	64.31		76.93	77.65	76.71	71.15	72.56	74.61	74.13	74.08	74.52	74.09	74.72	75.36	73.72	75.62	73.85	73.72	73.92					
Cr#	18.60	18.35	18.18	18.53	15.14	33.18	33.61	33.07	15.34	15.51	60.20	59.78	59.74		11.10	11.22	11.43	19.68	19.54	17.80	17.98	17.64	16.40	15.96	18.35	16.27	16.39	16.22	17.10	16.56	17.07					

	Harzburgites																														
Clinopyroxene	04OM63a2	04OM63a2	04OM63a2	04OM63a2	04OM63a2	04OM63a23	04OM63a2	04OM63a21	04OM63a22	04OM63a12	04OM63a1	04OM63a1	04OM63a1	04OM63a1	04OM63a1	04OM63c1	04OM62b1	04OM62b1	04OM62b1	04OM58b1	04OM58b1	04OM58b1	04OM63c3	04OM63c3	04OM63c3	04OM63c3	04OM63c3	04OM63c3			
SiO2	54.22	53.96	54.09	54.10	53.75	53.56	53.24	53.16	53.37	53.67	53.38	53.88	53.67	53.30	53.15	53.88	54.01	54.21	53.80	53.93	53.39	53.43	53.23	53.04	53.34	53.48	53.26	53.15			
TiO2	-	0.05	0.01	0.02	0.03	0.02	0.05	0.07	-	-	0.04	0.01	0.08	-	-	0.09	0.07	0.07	0.07	0.07	0.16	0.07	0.12	0.07	0.08	0.12	0.12	0.10			
Al2O3	2.58	2.84	2.59	2.85	2.62	2.53	2.77	2.79	2.57	2.96	2.95	2.90	2.69	2.82	2.86	3.55	2.57	2.52	2.59	3.61	3.62	3.87	4.43	4.42	4.28	4.25	4.23	4.45			
Cr2O3	0.55	0.53	0.56	0.45	0.32	0.46	0.36	0.50	0.44	0.46	0.51	0.46	0.39	0.40	0.50	0.99	1.51	1.59	1.60	0.93	0.94	0.94	0.73	0.70	0.73	0.82	0.74	0.66			
Fetot	1.98	2.01	2.14	2.22	2.13	2.08	2.00	2.04	2.15	2.33	2.27	2.34	2.13	2.18	2.35	2.14	2.56	2.46	2.56	2.35	2.43	2.33	2.42	2.26	2.32	2.29	2.32	2.39			
MnO	0.12	0.02	0.12	0.10	0.07	0.08	-	0.12	0.07	0.13	0.13	0.07	0.10	0.08	0.09	0.02	-	0.10	0.09	0.04	0.01	0.15	0.07	0.09	0.12	0.13	-	0.03			
MgO	16.98	16.83	17.14	17.01	17.16	16.79	16.70	16.83	16.77	16.66	16.76	16.82	16.69	16.75	16.96	16.36	17.52	17.53	17.58	16.49	16.30	16.14	16.04	16.09	15.98	15.99	15.94	15.83			
CaO	23.10	23.13	23.28	23.16	23.22	22.98	22.87	22.82	23.09	23.16	22.9	23.17	23.58	23.20	23.26	22.34	20.47	20.87	20.73	21.54	21.32	21.08	21.75	21.90	21.88	21.93	21.86	21.91			
Na2O	0.34	0.47	0.47	0.44	0.44	0.40	0.49	0.51	0.54	0.45	0.49	0.45	0.47	0.48	0.45	0.98	0.75	0.83	0.79	1.08	1.29	1.27	1.06	1.08	1.01	1.01	0.99	0.92			
Total	99.88	99.82	100.40	100.34	99.76	98.89	98.49	98.86	99.08	99.83	99.48	100.10	99.82	99.26	99.76	100.34	99.46	100.18	99.85	100.03	99.56	99.30	99.85	99.71	99.74	100.07	99.47	99.45			
Mg#	93.86	93.72	93.46	93.17	93.49	93.50	93.70	93.62	93.28	92.72	92.92	92.76	93.33	93.18	92.77	93.16	92.42	92.70	92.44	92.59	92.27	92.52	92.19	92.68	92.47	92.56	92.45	92.19			
	Lherzolites																														
Clinopyroxene	OM66d2	OM66d2	OM66d2	04OM58f3	04OM58f3	04OM58f3	04OM58f3	04OM58f3	04OM58f3	04OM58f3	04OM58f3	04OM63c2	04OM63c2	04OM63c2	04OM63c2	04OM63c2	04OM63c2	04OM63c2	04OM62b2	04OM62b2	04OM62b2	04OM62b2	04OM62b2	04OM62b2	04OM58a2	04OM58a2	04OM58a2	04OM58a2	04OM58a2	04OM58a2	04OM58a2
SiO2	52.23	52.28	52.58	52.57	52.23	52.47	51.94	51.95	52.63	52.57	52.69	51.93	52.12	51.69	52.17	52.41	52.63	52.68	52.10	51.74	51.75	51.22	51.67	51.93	52.37	52.36	52.22	52.14	52.09	51.94	51.53
TiO2	0.17	0.04	0.09	0.15	0.15	0.10	0.12	0.14	0.17	0.21	0.11	0.09	0.13	0.12	0.07	0.06	0.05	0.09	0.45	0.48	0.55	0.48	0.48	0.46	0.13	0.13	0.16	0.12	0.06	0.18	0.14
Al2O3	5.69	5.66	5.67	5.27	4.97	5.04	5.13	5.17	5.15	5.20	4.98	4.61	4.68	4.69	4.69	4.80	4.74	4.72	7.49	7.42	7.48	7.30	7.39	7.41	5.34	5.25	5.27	5.33	5.30	5.19	5.32
Cr2O3	1.04	1.05	1.02	0.86	0.84	0.81	0.90	0.82	0.85	0.76	0.71	0.70	0.69	0.65	0.77	0.76	0.83	0.68	0.88	0.80	0.89	0.87	0.85	0.87	0.95	0.89	0.77	0.84	0.81	0.82	0.82
Fetot	3.40	3.40	3.31	2.82	2.83	2.69	2.83	2.85	2.98	2.70	2.95	3.33	3.11	3.09	3.33	3.38	3.18	3.26	3.53	3.30	3.21	3.52	3.46	3.47	2.99	2.83	2.92	3.09	2.97	2.98	3.15
MnO	0.13	0.13	0.18	0.04	0.09	0.10	0.13	0.09	0.11	0.06	0.12	-	0.12	0.15	0.05	0.06	0.04	0.07	0.12	0.10	0.15	0.07	0.10	0.11	0.03	0.09	0.12	0.01	0.09	0.08	0.06
MgO	15.79	15.84	15.69	16.36	16.24	16.09	15.85	16.08	15.88	16.09	16.24	16.04	15.94	16.15	16.00	15.80	15.99	16.05	15.75	15.73	15.60	15.66	15.45	15.61	16.26	16.25	16.22	15.90	16.15	16.24	15.86
CaO	20.21	19.99	20.28	21.09	21.28	21.13	20.96	21.29	21.30	21.24	21.31	21.01	21.02	21.51	21.32	21.52	21.52	21.47	18.54	18.81	18.85	18.70	18.39	18.80	20.77	20.97	20.90	21.00	20.95	20.95	21.07
Na2O	1.38	1.38	1.51	1.05	1.01	1.04	1.05	1.09	1.09	1.07	1.01	0.81	0.78	0.87	0.80	0.92	0.72	0.84	1.67	1.53	1.63	1.58	1.48	1.62	1.19	1.06	1.03	1.11	1.10	1.09	1.06
Total	100.18	99.90	100.49	100.31	99.78	99.52	98.97	99.70	100.23	99.96	100.24	98.58	98.57	99.11	99.27	99.78	99.70	99.90	100.59	99.96	100.17	99.54	99.27	100.38	100.19	99.93	99.73	99.67	99.69	99.64	99.21
Mg#	89.23	89.26	89.42	91.18	91.09	91.42	90.89	90.94	90.48	91.40	90.76	89.56	90.13	90.31	89.53	89.28	89.96	89.76	88.82	89.45	89.66	88.79	88.83	88.90	90.65	91.09	90.81	90.15	90.65	90.67	89.97
	Lherzolites																														
Clinopyroxene	04OM58c3	04OM58c3	04OM58c3	04OM58c3	04OM59b2	04OM59b2	04OM59b2	04OM59b2	04OM59b2	04OM59b2	04OM59b2	04OM58a3	04OM58a3	04OM58a3	04OM58a3	04OM58a3	04OM58a3														
SiO2	52.85	53.23	52.91	53.04	52.26	52.91	52.38	52.34	52.77	52.23	52.68	52.15	51.64	51.73	51.87	51.97	51.97														
TiO2	0.11	0.17	0.15	0.21	0.10	0.09	0.15	0.13	0.10	0.10	0.09	0.13	0.13	0.11	0.05	0.14	0.11														
Al2O3	5.23	5.27	5.19	5.10	5.24	4.99	4.83	5.00	5.00	4.81	4.94	5.71	5.77	5.74	5.78	5.82	5.71														
Cr2O3	0.96	0.86	0.92	0.89	0.93	0.66	0.75	0.70	0.73	0.76	0.74	0.94	1.00	0.92	0.90	0.89	0.88														
Fetot	2.80	2.72	2.93	2.82	3.06	3.07	3.03	3.07	2.91	2.95	3.02	3.21	3.06	3.06	3.18	3.25	3.37														
MnO	0.06	0.08	0.07	0.07	0.09	0.13	0.05	-	0.08	0.13	0.06	0.04	0.16	0.04	0.13	0.07	0.11														
MgO	16.08	16.02	15.87	15.96	16.15	16.38	16.07	16.55	16.39	16.05	16.15	16.05	16.08	16.09	15.84	16.12	16.18														
CaO	21.12	21.02	20.92	21.08	20.98	21.00	21.04	20.51	21.35	21.15	21.20	20.53	20.51	20.31	20.38	20.37	20.48														
Na2O	1.08	1.14	1.07	1.12	0.91	0.92	0.90	0.83	0.93	0.94	0.92	1.10	1.16	1.19	1.09	1.16	1.15														
Total	100.35	100.53	100.02	100.31	99.77	100.18	99.22	99.12	100.35	99.23	99.85	99.95	99.71	99.34	99.30	99.94	100.17														
Mg#	91.09	91.30	90.61	90.98	90.39	90.47	90.44	90.57	90.93	90.64	90.50	89.90	90.35	90.36	89.88	89.84	89.53														

Table 2

Click here to download Table: Table 2.xls

	Harzburgites			Lherzolites								
Clinopyroxene	**04OM63c3**	**04OM63c1**	**04OM62b1**	**04OM58c3**	**04OM59b2**	**04OM58f3**	**04OM62b2**	**04OM58a2**	**04OM58a3**	**04OM58c1**	**04OM63c2**	**04OM66d2**
	n=4	**n=3**	**n=3**	**n=5**	**n=3**	**n=3**	**n=4**	**n=5**	**n=4**	**n=4**	**n=3**	**n=3**
Sc	97	91	63	76	69	70	68	71	62	97	55	66
Ti	945	569	722	1008	851	1154	3482	950	755	701	718	846
V	244	243	181	232	246	222	258	241	244	287	186	258
Ni	403	310	381	270	291	300	324	364	317	318	262	311
Rb	0.80	0.80	**bdl**	**bdl**	**bdl**	1.55	**bdl**	1.00	0.62	0.26	0.66	1.86
Sr	61	273	254	76	75	65	79	456	183	83	296	313
Y	14	14	4	12	12	14	24	13	13	13	10	13
Zr	1.23	3.69	28	1.63	0.52	1.98	40	0.68	4.58	0.76	12	18
Nb	0.38	1.34	1.36	0.59	2.23	1.44	0.21	0.88	3.61	**bdl**	0.30	3.56
Ba	1.34	1.66	0.43	0.34	0.61	0.44	0.96	1.55	0.52	0.40	0.74	7.4
La	6.0	25	6.5	8.9	9.7	7.3	1.00	37	32	47	50	39
Ce	4.41	46	15	11	14	9.5	3.49	53	42	75	46	71
Pr	0.18	4.92	2.03	0.95	1.20	0.87	0.73	3.61	3.33	5.9	3.26	7.1
Nd	0.69	16	9.4	3.08	3.63	3.16	4.43	8.0	9.63	14	8.4	24
Sm	0.32	3.40	2.69	0.69	0.75	0.72	1.80	1.29	1.50	1.89	1.31	5.38
Eu	**bdl**	0.94	0.91	0.29	0.22	0.28	0.79	0.38	0.41	0.53	0.37	1.32
Gd	0.99	2.78	2.56	1.26	1.00	1.36	3.13	1.17	1.22	1.47	1.24	3.15
Dy	1.98	2.53	2.32	1.96	1.58	2.13	3.94	1.69	1.59	1.95	1.69	2.42
Ho	0.52	0.50	0.34	0.49	0.39	0.50	0.88	0.41	0.40	0.46	0.38	0.47
Er	1.58	1.45	0.70	1.48	1.16	1.49	2.48	1.30	1.29	1.44	1.15	1.34
Yb	1.59	1.30	0.48	1.51	1.17	1.48	2.38	1.40	1.35	1.48	1.13	1.28
Lu	0.23	0.20	0.05	0.23	0.17	0.22	0.34	0.21	0.20	0.23	0.17	0.20
Hf	0.17	0.25	0.77	0.18	0.14	0.20	1.34	0.27	**bdl**	0.16	0.53	0.82
Th	1.82	3.45	0.36	3.12	1.44	1.29	0.02	4.28	6.31	5.32	13	2.17
U	0.44	0.57	0.07	0.77	0.24	0.25	0.01	0.72	0.64	0.81	3.12	0.44

bdl: below detection limit